TU/e EINDHOVEN UNIVERSITY OF TECHNOLOGY

Multi-scale simulations for predicting materials properties of a cross-linked polymer

Citation for published version (APA):
Kacar, G., Peters, E. A. J. F., & With, de, G. (2015). Multi-scale simulations for predicting materials properties of a cross-linked polymer. *Computational Materials Science*, *102*, 68-77. https://doi.org/10.1016/j.commatsci.2015.02.021

DOI:
10.1016/j.commatsci.2015.02.021

Document status and date:
Published: 01/01/2015

Document Version:
Publisher's PDF, also known as Version of Record (includes final page, issue and volume numbers)

Please check the document version of this publication:

• A submitted manuscript is the version of the article upon submission and before peer-review. There can be important differences between the submitted version and the official published version of record. People interested in the research are advised to contact the author for the final version of the publication, or visit the DOI to the publisher's website.
• The final author version and the galley proof are versions of the publication after peer review.
• The final published version features the final layout of the paper including the volume, issue and page numbers.

Link to publication

General rights
Copyright and moral rights for the publications made accessible in the public portal are retained by the authors and/or other copyright owners and it is a condition of accessing publications that users recognise and abide by the legal requirements associated with these rights.

• Users may download and print one copy of any publication from the public portal for the purpose of private study or research.
• You may not further distribute the material or use it for any profit-making activity or commercial gain
• You may freely distribute the URL identifying the publication in the public portal.

If the publication is distributed under the terms of Article 25fa of the Dutch Copyright Act, indicated by the "Taverne" license above, please follow below link for the End User Agreement:

www.tue.nl/taverne

Take down policy
If you believe that this document breaches copyright please contact us at:

openaccess@tue.nl

providing details and we will investigate your claim.

Download date: 17. Nov. 2023

Computational Materials Science 102 (2015) 68–77

Contents lists available at ScienceDirect

Computational Materials Science

journal homepage: www.elsevier.com/locate/commatsci

Multi-scale simulations for predicting material properties of a cross-linked polymer

Gokhan Kacar, Elias A.J.F. Peters, Gijsbertus de With *

Laboratory of Materials and Interface Chemistry, Department of Chemical Engineering and Chemistry, Eindhoven University of Technology, Eindhoven, The Netherlands

ARTICLE INFO

Article history:
Received 21 November 2014
Received in revised form 3 February 2015
Accepted 11 February 2015

Keywords:
Multi-scale
Reverse-mapping
DPD
MD
Material properties
Polymer

ABSTRACT

In this paper we aim at predicting material properties of a cross-linked polymer by using multi-scale simulations and to compare the elastic properties and glass transition temperature with experimentally observed values. To that purpose we use an epoxy polymer for which the starting point is a mesoscopic simulation of its cross-linked structure realized by Dissipative Particle Dynamics (DPD) simulations, as recently improved to conserve local densities properly. This results in a coarse-grained structure of this thermoset polymer, relaxed at a large length- and long time-scale. Such a mesoscopic simulation is important as otherwise insufficient relaxation of the structures occurs for a later and proper comparison with experimental properties. Allowing further simulations at the atomistic scale using molecular dynamics (or any other method) to obtain material properties, a reverse-mapping procedure is required to insert atomistic detail into the coarse-grained structures. Hence, an efficient and reliable reverse-mapping procedure was implemented to be able to connect these two types of simulation. For the epoxy polymer chosen, Poisson's ratio, the elastic modulus, the glass transition temperature and the thermal expansion coefficients of the glassy and rubbery state resulting from the equilibrated reverse-mapped structure, match the experimental values well. Overall, the paper reports a fast and straightforward procedure to bridge a mesoscopic structure to experimentally observed material properties, which can be applied to any system of interest.

© 2015 Elsevier B.V. All rights reserved.

1. Introduction

Epoxies are widely used in coatings, electronic, paint, marine, and aerospace industries. The structure formation of these epoxies is due to a complex cross-linking process in which chemical reactions between monomers and reconfiguration of monomers and already cross-linked chains take place. For a proper understanding of their structure and properties, exploration of the molecular behavior of these epoxies on a wide range of time and length scales is needed. One of the commonly employed simulation tools for studying materials at smaller time scales is the molecular dynamics (MD) approach [1]. However, reaching the time scales necessary to reach a sufficiently relaxed and cross-linked polymer is currently unfeasible with conventional MD simulations. To create cross-linked polymeric structures at the atomistic resolution is computationally expensive as the reactive groups diffuse slowly due to the long relaxation times. Attempts to overcome such type of intrinsic time-scale problems are often made by introducing algorithms that bring the functional groups in close proximity to increase the reaction rate [2]. A high conversion rate might be reached, but on the other hand, this would induce internal stresses which at the end might require even longer times to relax the cross-linked polymer. Therefore, to create and relax the cross-linked structure, calculations at the intermediate meso-scale level are required [2–7]. To this end, we recently performed meso-scale Dissipative Particle Dynamics (DPD) [8,9] simulations for the cross-linked structure of an experimentally studied epoxy [10,11].

After having created the equilibrium mesoscopic cross-linked structure of a polymer, a possible route for further investigation is to compute material properties such that a direct comparison with the experimental values can be done. For this purpose one can consider, for example, a combination of DPD and Lattice spring model [12] or a multi-scale approach by means of atomistic simulations from reverse-mapped coordinates of DPD. We opt to continue with the second choice as it covers a more general approach, and also avoids many (not easily solved) problems, such as representing the interactions necessary to quantify the material properties at meso-scale. In this paper we report an efficient and reliable reverse-mapping (or fine-graining) procedure generating a reasonably well equilibrated relaxed structure and apply this procedure to the bulk epoxy created mesoscopically (see Ref.

* Corresponding author.
E-mail address: g.dewith@tue.nl (G. de With).

http://dx.doi.org/10.1016/j.commatsci.2015.02.021
0927-0256/© 2015 Elsevier B.V. All rights reserved.

[10]) in order to generate the atomistic coordinates to perform atomistic simulations. The need for reverse-mapping will be clear: In a coarse-grained description a large number of the degrees of freedom, such as the spatial rotations or translational mobility of the representative atomistic units are lost; however, to perform all-atom simulations, the proper atomistic structure (i.e., the detailed coordinates of the atoms) of a coarse-grained entity should be known. Finding a proper solution is not straightforward as a number of atomistic configurations within a coarse-grained entity are possible. For instance, one procedure is the fitting of atomistic templates (representative atomistic representations of the corresponding coarse-grained entities) using only two constraints: (i) the center-of-mass (CoM) of the atomistic configuration and of the coarse-grained beads are the same; and (ii) a proper connectivity is realized. Here, to improve the fitting procedure, certain rotation operations for these templates are applied for realizing a lower energy structure. As an alternative procedure, it can be attempted to fit the whole representative all-atom chain configuration to its coarse-grained counterpart. After fitting procedure, methods such as steepest descent, conjugate gradient, Newton–Raphson [1], or a combination of these, could be applied to energy minimize the fitted structures. These are the steps that can be found in various applications of reverse-mapping procedures in the literature [13–20].

After having obtained the atomistic coordinates *via* the reverse-mapping procedure, we perform all-atom MD simulations to compute the elastic properties of the bulk cross-linked epoxy. Various methods are available for estimating the stiffness matrix elements from strain fluctuations such as the constant-strain minimization method [21], which induces infinitesimal stresses to deform the box, or the Parinello-Rahman [22] approach that employs a constant stress ensemble. Here, we estimate the elastic modulus E and Poisson's ratio v directly from the cross-correlations in the box fluctuations at zero external pressure. The required expressions are derived following the route as employed in standard fluctuation theory [23]. Moreover, we compute the glass transition temperature T_g. As the polymer is cooled down, a transition from the rubber-like state to a glassy state is observed. In simulations, this transition can be monitored by evaluating different properties of the material, such as heat capacity, mean squared displacement, Young's modulus, density, and volume. If these are plotted versus temperature, the decreasing trend upon quenching differs in the glass and amorphous regimes. Here we use the volume of the material plotted with respect to the temperature to estimate T_g. As a by-product the thermal expansion coefficients of the glassy and rubbery state were estimated. For all properties, the computed values are compared with the ones reported in the literature.

2. Computational details

2.1. Mesoscopic creation of bulk epoxy structure

The epoxy studied consists of a DGEBA (Diglycidylether-Bisphenol-A) pre-polymer and DETA (Diethylene-Tri-Amine) as cross-linker (Fig. 1). The DGEBA is two-functional monomer as it has two reactive epoxy groups, whereas the DETA is five-functional. Therefore, a stoichiometric 1:1 ratio of functional groups is composed of a 5:2 molar ratio.

The epoxy network is created at the meso-scale by performing DPD simulations, as described previously [10]. In brief, the cross-link reactions are based on a statistical procedure where two cross-linking beads are connected with a covalent bond if they approach each other within a pre-defined distance using a step function. By this procedure we obtained 92% cross-link conversion. The network obtained is essentially independent of the precise distance chosen as well of the shape of the cross-linking function, as shown in Ref. [24] using a hyperbolic tangent function instead of a step function.

DPD has proven to be a useful method in representing polymer behavior. The defined interactions between coarse-grained entities (often referred as beads) are mapped from the experimental thermodynamic quantities [8,25] and the method describes the hydrodynamic behavior correctly, which is crucial in simulating longer time-scales. Conventionally, these beads are assumed to have similar volumes. However, beads are usually chosen to represent chemical groups, which obviously have different volumes. Therefore, in a recent study, we incorporated the variable volume effect into the DPD parameterization still preserving the Groot–Warren formalism, but extending the method to represent experimental pure-liquid volumes of beads in the simulations [26]. Having the correct volumes of the beads is crucial during the cross-linking as reacting beads are finding each other as the simulation progresses. Moreover, in attempts of reverse-mapping, similarly as targeted here, the local density variations in the system should be properly modeled. In this paper we use exactly the same definitions of interactions, simulation parameters, and the end-structure as reported before and refer the reader to reference [10] for the mesoscopic simulation details. We use the same spatial coordinates as generated in the aforementioned study, and applied a fast and efficient reverse-mapping algorithm of which the details are given in the Section 2.3.

2.2. Atomistic simulation details

Atomistic simulations of the reverse-mapped structure are performed. The all-atom simulations are run with the LAMMPS code [27] using the PCFF (Polymer Consistent Force Field) [28] which has the functional form of a class II force field [29], and is developed specifically for polymers and organic materials.

As a first step the total energy of the reverse-mapped cross-linked bulk epoxy structure is minimized by iteratively adjusting the atomistic coordinates until the change in energy is less than 10^{-6} kcal/mol. The structure is relaxed in an *NPT* ensemble with a small time step of 0.1 fs for 500 ps. Thereafter, a 6 ns production run is performed with a 1 fs time step. Data is evaluated between 2 ns and 6 ns of the production run. The thermostat is selected as Nosé-Hoover [30,31], the pressure control is performed by Parinello-Rahman [32] barostat while all simulations are performed at room temperature and 1 atm pressure. Pressure control is set in all dimensions and the box fluctuations are coupled in horizontal (x and y) but uncoupled in vertical (z) dimension. This ensures that the instantaneous change in box length of x and y dimensions are equal, and unequal in z dimension. For the electrostatic contribution the particle-mesh Ewald (PME) [33] summation is used. For Lennard-Jones interactions a cut-off distance of 10 Å is used. The system consists of 20,850 atoms using a periodic box with initial dimensions in xyz as 56.8 Å, 57.5 Å, and 72.5 Å. The initial dimensions of x and y directions are different as the reverse-mapped structure is later used in modeling the interactions with a metal-oxide surface.

To estimate T_g, we evaluated the equilibrium volumes at various temperatures from relaxed structures, obtained from atomistic *NPT* simulations performed at 1 atm external pressure. All the simulation parameters are set as mentioned in the previous section, and we started with the relaxed structure as obtained in the previous section. Initially, we increase the temperature to 600 K, which is significantly above the experimental T_g. Then, in a stepwise fashion, we cool down to 300 K with steps of 15 K. The cooling rate between discrete steps corresponds to 15 K/500 ps. After each step, the structures were energy minimized (for 100 ps using a time step of 0.1 ps) and further production runs (of duration 2 ns using a time step of 1 ps) were carried out, similar as before.

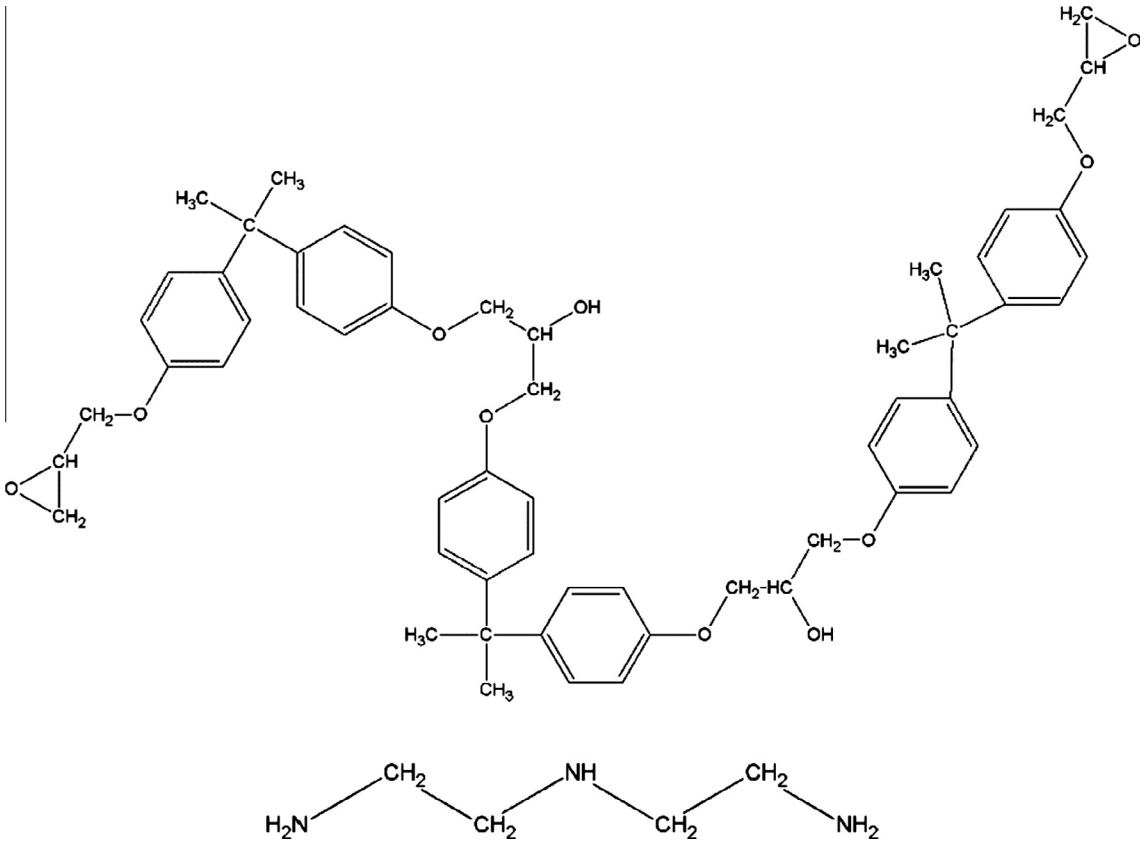

Fig. 1. Schematic representation of DGEBA and DETA chains.

2.3. Reverse-mapping

In a reverse-mapping procedure, as mentioned in the introduction, a usual first step is fitting of the atomistic coordinates from a library of templates to the mesoscopic coordinates. However, it is quite likely that such a step leads to a wide distribution of the back-bone bond lengths as the templates are oriented differently with respect to each other. This is illustrated in the schematic representation Fig. 2a, where randomly oriented templates are represented as vectors. Hence, bond lengths may significantly deviate from their equilibrium values, being either too large or too small. Such type of configurations will result in a high energy structure and the energy minimization will be time consuming since the number of iteration steps is proportional to how far the bond lengths deviate from their equilibrium values. So if, with some procedure, the templates are rotated such that the sum of all the bond lengths of the main back-bone is decreased, this would be a great benefit in the later energy minimization.

In this paper, we present a straightforward, yet fast and efficient atomistic detail mapping algorithm that aligns the templates in such a way that they become ordered within a particular chain, as depicted in Fig. 2b. Thus, the sum of bond lengths will be smaller and the corresponding energy minimization will take less computational effort as compared to a structure composed of randomly oriented templates.

To perform the alignment, characteristic vectors $\mathbf{c}_j$ are introduced for each of the templates labeled j, defined as the arrows for the CoM of the templates to the atom that connects consecutive templates. Obviously, these characteristic vectors are template-specific, and an example of how these vectors are defined for two different templates is given in Fig. 2c.

The method applied is a modified version of a previously established one [34,35], where the rotation between templates was based on the angle between consecutive templates. Here, we changed the rotation procedure by aligning the characteristic vectors defined for each template in parallel directions, rendering a very fast reverse-mapping procedure, yet diminishing the sum of all the bond lengths of the main back-bone significantly. The main components of the algorithm used here are the rotation (or alignment) and translation steps. In the rotation step, the aim is to provide a reasonably well pre-equilibrated structure before proceeding with the energy minimization. Thereafter, the rotated templates are translated to the MD coordinates, followed by an energy minimization for the whole structure.

The algorithm operates as follows:

(1) Compute the CoM and translate the templates so that their CoMs superimpose at the origin.
(2) Define a characteristic vector for each template.
(3) By using the characteristic vectors compute a rotation matrix.
(4) With this rotation matrix perform a rotation for each template and translate to the coarse-grained coordinates.
(5) Check the bond length between successive templates to see if the value is below a pre-defined value.
(6) Update coordinates and iterate from step 3 if step 5 is not satisfied.
(7) Perform step 1 till step 6 for all templates consecutively in all chains.
(8) Energy minimize the whole structure.

The first step is a straightforward one. Computing the CoMs of the templates is finding the mass-weighted averages of coordinates according to

$$r_{CoM} = \frac{1}{M}\sum_i m_i r_i, \quad r = [x, y, z] \tag{1}$$

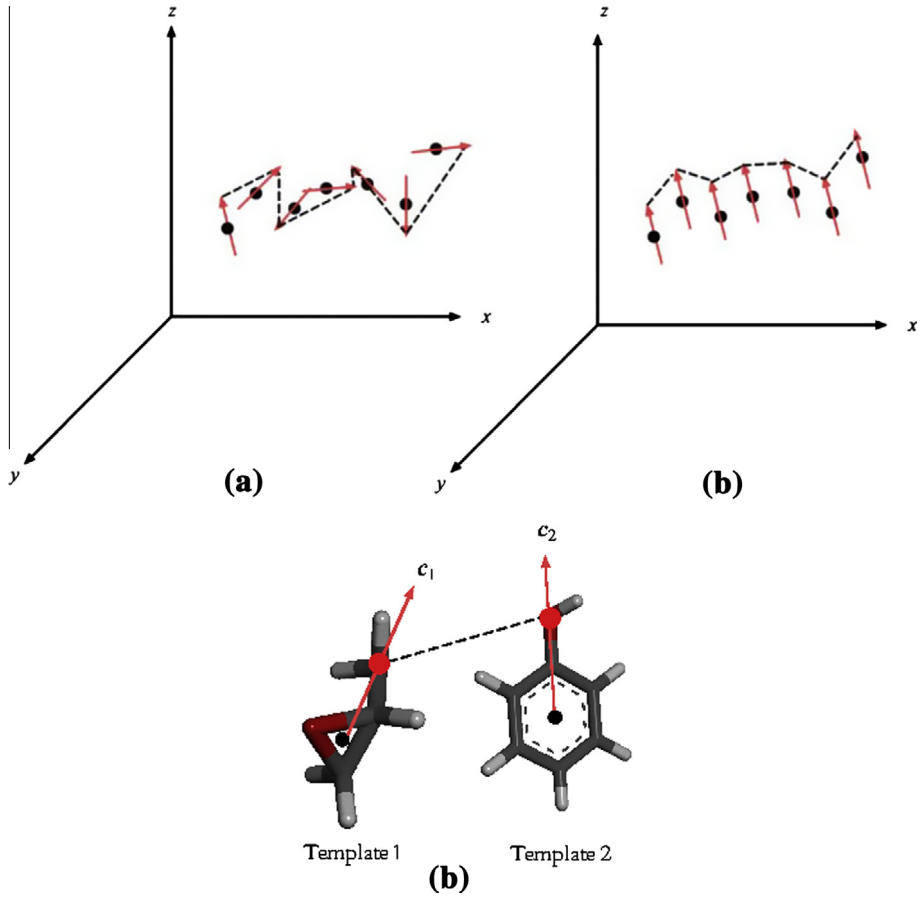

Fig. 2. (a) A set of randomly oriented characteristic vectors, (b) characteristic vectors aligned to orient in the same direction, and (c) demonstrating how the characteristic vectors c_j are defined. The dashed line stands for the bond between these templates while the filled circles (●) represent the mesoscopic coordinates to which the templates are translated.

where M is the total mass of the template, and m_i and are r_i are the mass and coordinates of the constitutive atom i of the template, respectively, while in the translation part, the CoM of each template is subtracted from the coordinates of the atoms so that their CoM is at the origin:

$$r_{i,new} = r_i - r_{CoM} \tag{2}$$

In the second step, the rotation operation aligns the templates in a chain in parallel directions. The rotation procedure adapted from the work as reported by Dollase [36] and based on the computation of a rotation matrix. In our case, we align the characteristic vectors $\boldsymbol{c}_j$ defined for each template, as depicted in Fig. 2. In this case the matrix equation to be solved is

$$\boldsymbol{c}_j^{(fixed)} = \boldsymbol{R}\boldsymbol{c}_j^{(1)} \tag{3}$$

Here, $\boldsymbol{c}_j^{(fixed)}$ remains fixed, as it describes the parallel direction, and $\boldsymbol{c}_j^{(1)}$ is rotated by the rotation matrix $\boldsymbol{R}$, given by

$$\boldsymbol{R} = \begin{bmatrix} l^2+(1-l^2)\cos\theta & lm+(1-\cos\theta)-n\sin\theta & nl(1-\cos\theta)+m\sin\theta \\ ml(1-\cos\theta)+n\sin\theta & m^2+(1-m^2)\cos\theta & mn(1-\cos\theta)-l\sin\theta \\ nl(1-\cos\theta)-m\sin\theta & mn(1-\cos\theta)+l\sin\theta & n^2+(1-n^2)\cos\theta \end{bmatrix} \tag{4}$$

where l, m, n are the direction cosines and θ provides a counter-clockwise rotation. Solving Eq. (3) characterizes the $\boldsymbol{R}$ matrix for the best fit. For this we use an iterative minimization procedure using a linearized $\boldsymbol{R}$ matrix, denoted by $\boldsymbol{S}$, and which follows a procedure called small angle rotation [37]. If the angle of rotation is small, then $\cos\theta \approx 1$ and $\sin\theta \approx \theta$, and $\boldsymbol{R}$ can be approximated by

$$\boldsymbol{R} \cong \boldsymbol{S} = \begin{bmatrix} 1 & -n\theta & m\theta \\ n\theta & 1 & -l\theta \\ -m\theta & l\theta & 1 \end{bmatrix} \tag{5}$$

with this approximation Eq. (3) can be written as $\boldsymbol{c}_j^{(fixed)} = \boldsymbol{S}\boldsymbol{c}_j^{(k)}$ in which the superscript (k) indicates an iteration number and where for the initial value we take $\boldsymbol{c}_j^{(1)}$, as obtained from the CoM matching only. Using the least-squares method we minimize $[\boldsymbol{c}_j^{(fixed)} - \boldsymbol{c}_j^{(k)}]^2$. Rearranging we obtain

$$\begin{bmatrix} c_{j,x}^{(fixed)} - c_{j,x}^{(k)} \\ c_{j,y}^{(fixed)} - c_{j,y}^{(k)} \\ c_{j,z}^{(fixed)} - c_{j,z}^{(k)} \end{bmatrix} = \begin{bmatrix} 0 & c_{j,z}^{(k)} & -c_{j,y}^{(k)} \\ -c_{j,z}^{(k)} & 0 & c_{j,x}^{(k)} \\ c_{j,y}^{(k)} & -c_{j,x}^{(k)} & 0 \end{bmatrix} \begin{bmatrix} l\theta \\ m\theta \\ n\theta \end{bmatrix} \tag{6}$$

or $\boldsymbol{Y} = \boldsymbol{C}\boldsymbol{P}$ in short. To solve this matrix equation for $\boldsymbol{P}$, we use one of the procedures to compute a 'best-fit' solution to system of linear equations that lacks a unique solution, called the Moore–Penrose pseudoinverse formalism [38,39], which yields

$$\boldsymbol{P} = (\boldsymbol{C}^T\boldsymbol{C})^{-1}\boldsymbol{C}^T\boldsymbol{Y} \tag{7}$$

From Eqs. (6) and (7) the rotation parameters can then be extracted as

$$\theta = \{(l\theta)^2 + (m\theta)^2 + (n\theta)^2\}^{1/2}, \quad l = (l\theta)/\theta, \quad m = (m\theta)/\theta, \quad n = (n\theta)/\theta \tag{8}$$

By using these parameters, the $\boldsymbol{R}$ matrix in Eq. (3) can be constructed to be employed in calculating all atomistic coordinates of the template, and the procedure is repeated for all templates. Please note that this rotation should be considered as a rigid rotation of the entire set (of atoms in a template). Moreover, a scaling factor of 7.15 Å is used as derived in Ref. [10] for conversion of DPD units to the physical values. After the templates are rotated and carried to the atomistic coordinates, the bond length between two sequential templates is calculated. If the distance of a new bond is below a predefined value, chosen here as 2.5 Å, the iteration stops to prevent further (and unnecessary) rotation. This value is selected to be higher than a typical bond length to prevent subtleties in the algorithm. After the algorithm is run for all consecutive pairs, the computed rotation matrix is used to rotate all the templates. Finally, the translation to the meso-scale coordinates is performed following an energy minimization of the whole structure.

3. Results and discussion

As the structure of an epoxy as simulated by DPD has been discussed before [40], we focus here on the reverse-mapping and the properties resulting from the reverse-mapped structure, as evaluated by MD.

3.1. Reverse-mapping

We first tested the reverse-mapping algorithm for a single epoxy chain (Fig. 3a), and thereafter the complete bulk epoxy (Fig. 3b). To assess the results, the distributions of the main chain bond lengths are plotted in Fig. 3 for three cases: (i) for templates fitted from the library of template coordinates only; (ii) for templates rotated as described; and (iii) for the resulting atomistic structures energy minimized.

The bond length distribution after merely fitting shows a rather unrealistic bond length distribution with bond lengths ranging from 2 to 6 Å. Clearly, aligning the templates in similar directions provides a much more realistic bond length distribution with bond lengths ranging from 1 to 2.5 Å. As the aligned structure is further energy minimized, the tail of the histograms corresponding to bond lengths larger than 2 Å is almost zero. The width of the bond length distributions, especially for a single chain, results from lack of statistics and variability of bond length within a chain. Occasionally, there are values which are unrealistically high. These long bonds correspond to the cross-links between different chains in the epoxy. The algorithm applied obviously does not 'correct' bond lengths between different chains, but these bonds will be easily 'corrected' during the energy minimization step since the number of cross-link bonds is much less as compared to the number of bonds in between different templates. Moreover, most of the bonds that deviate from their equilibrium values are over-stretched bonds that originate from the raw-fitted coordinates. These bonds are partially corrected in the rotation step, but a minor portion of these bonds corresponding to cross-links still remain. As the structures are further processed using the energy minimization, these long-bonds are fully corrected.

To further assess the algorithm, two separate sets of simulations are run: One with starting configurations taken from the structures of fitted library of templates and one with the rotation algorithm is applied. We show in Fig. 4a the total energy as a function of simulation time associated with the energy minimization performed at 0 K. The initial discrepancy in the total energy values are significantly different from each other and the energy minimizations are observed to be quite fast in both of the systems. For longer times Fig. 4b depicts that the total energy values for both cases show a fast decay initially. To further analyze, we fitted a power law equation to the total energies. It is observed that if we continue to relax the structures, the power law fits indicate that both of the structures from initial fit of templates and rotated templates seems to settle down, while the rotation of templates leads to significantly lower energy values. The difference in the final energy values is around 4.1% as realized from fit parameters. We repeated these calculations for two extra of different initial structures taken from different snapshots of a fully cross-linked reverse-mapped epoxy system (Fig. 4c and d). Even for a shorter simulation time of 1 ns, we observed from the power law fits that the total energies of the reverse-mapped structures rotated templates are smaller than the initial fit of templates with difference of 5% and 2%. A possible reason for this might be that the structure without rotation applied is stuck in a local energy minima. As the epoxy structure contains benzene rings, reverse-mapping procedure with randomly oriented templates might result in molecular interlocking effects, or ring inter-penetrations, which is impossible to be fixed for a classical MD simulation. The results clearly indicate that our proposed reverse-mapping approach not only provides a fast mapping of the atomistic detail to coarse-grained coordinates, but also improves the relaxation procedure by reaching lower total energy values while possibly correcting the molecular inter-locking effects as clearly visible from the total energies.

A typical example of the resulting atomistic configuration of the bulk epoxy after application of the reverse-mapping algorithm is depicted in Fig. 5a. The density profiles plotted for the different directions in the box show no systematic trend with direction and the fluctuations are due to statistics. Therefore, we assume that the epoxy network is isotropic.

3.2. Elastic properties of bulk epoxy

In this section we discuss the results of the atomistic simulations for the elastic properties of the bulk epoxy. The simulations are performed in the *NPT* ensemble where the box dimensions are allowed to change independently of each other, but the box shape remains rectangular. The goal is to obtain the elastic constants, elastic modulus E and Poisson's ratio ν, from the shape fluctuations of a simulation box, by using standard fluctuation theory [23].

The bulk epoxy can be assumed to be an isotropic material. If we consider normal stresses only, i.e., tensile and compressive but no shear stresses, and also assume that we are in the linear elastic regime, then Hooke's law

$$\varepsilon_i = \frac{1}{E}\left[\sigma_i(1+\nu) - \nu(\sigma_x+\sigma_y+\sigma_z)\right] \tag{9}$$

is valid, where σ_i and ε_i are the stress and strain in the x, y or z directions, respectively.

In an *NPT* simulation the number of particles, pressure and temperature are constant. Here the pressure and temperature are set by the external thermostat and barostat, respectively. We will consider a somewhat generalized setup where in each of the three directions an independent normal stress can be set. The thermodynamic potential that is relevant for these control variables is the Gibbs energy $G(N,T,\sigma_x,\sigma_y,\sigma_z)$. Since the situation that will be considered is at constant temperature and constant number of particles, only the variation with respect to the externally applied stresses is considered here and the variation with temperature and amount of particles is not discussed. So, keeping the notation compact, we discuss $G = G(N,T,\sigma_x,\sigma_y,\sigma_z) - G(N,T,0,0,0)$ and to obtain this quantity from Eq. (9), we integrate with respect to the three strains resulting in

$$dG = -\overline{V}\sum_i \varepsilon_i d\sigma_i \rightarrow G = \frac{-\overline{V}}{2E}\left[\left(\sigma_x^2+\sigma_y^2+\sigma_z^2\right) - 2\nu(\sigma_x\sigma_y+\sigma_x\sigma_z+\sigma_y\sigma_z)\right] \tag{10}$$

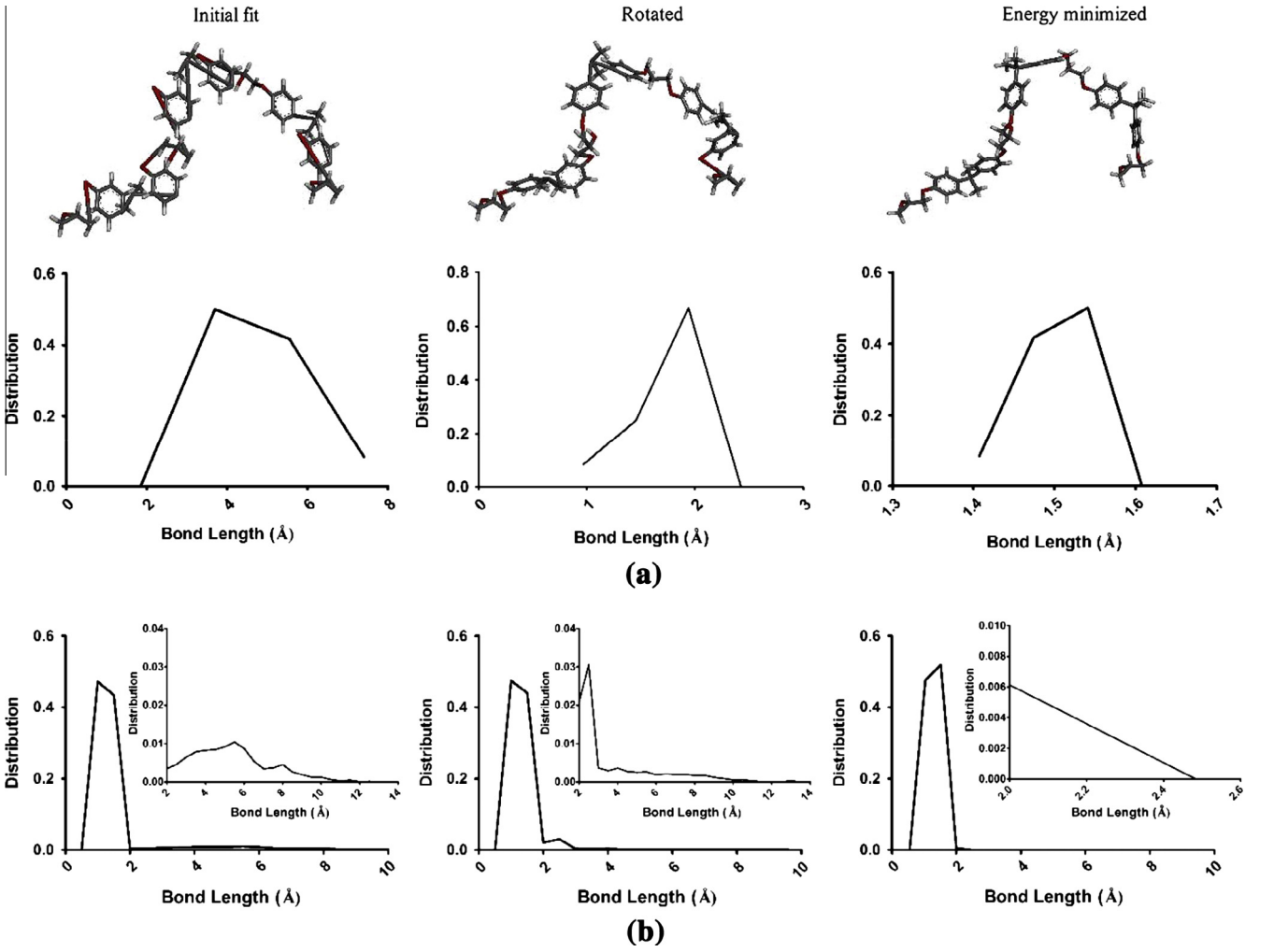

Fig. 3. The distribution of bond lengths after different steps are applied: templates are fitted from a library of template coordinates, rotated in parallel, and energy minimized for (a) a single epoxy chain, and (b) the whole cross-linked epoxy structure. The insets show a zoom-in of the main plots of (b) in order to depict the less visible tails. Above the histograms of (a), the configurations of a particular chain after each step are depicted.

In this equation $\overline{V}$ is the volume of the box at zero external stresses, i.e., if L_i is the size of the box in the i-direction and $\bar{L}_i$ its average value at zero tension (in all directions), then $\overline{V} \equiv \bar{L}_x \bar{L}_y \bar{L}_z$. Using the quantities L_i and $\bar{L}_i$, the small-deformation strains ε_i are defined as

$$\varepsilon_i = \frac{L_i - \bar{L}_i}{\bar{L}_i} \tag{11}$$

The second order derivatives of G are related to the elastic constants via

$$\frac{\partial^2 G}{\partial \sigma_i^2} = -\frac{\overline{V}}{E}, \quad \frac{\partial^2 G}{\partial \sigma_i \partial \sigma_j} = \frac{\overline{V} v}{E}, i \neq j \tag{12}$$

Calculating the (inverse) bulk modulus $B^{-1} = -V^{-1}\partial V/\partial p$, meanwhile using the relations $V = \overline{V}(1+\varepsilon_x)(1+\varepsilon_y)(1+\varepsilon_z)$ and $\sigma_x = \sigma_y = \sigma_z = -p$, results in

$$\frac{1}{B} = \sum_i \sum_j \frac{\partial \varepsilon_i}{\partial \sigma_j} = -\frac{1}{\overline{V}} \sum_i \sum_j \frac{\partial^2 G}{\partial \sigma_i \partial \sigma_j} = \frac{3(1-2v)}{E} \tag{13}$$

as expected for the bulk modulus for homogenous isotropic materials. From statistical mechanical considerations about fluctuations of the box size (see Appendix) we have

$$\begin{aligned} -vE^{-1} &= \frac{\overline{V}}{k_B T} \langle (\varepsilon_w - \langle \varepsilon_w \rangle)(\varepsilon_z - \langle \varepsilon_z \rangle) \rangle, \\ E^{-1} &= \frac{\overline{V}}{k_B T} \langle (\varepsilon_z - \langle \varepsilon_z \rangle)^2 \rangle, \end{aligned} \tag{14}$$

$$v = -\frac{\langle (\varepsilon_w - \langle \varepsilon_w \rangle)(\varepsilon_z - \langle \varepsilon_z \rangle) \rangle}{\left\langle (\varepsilon_z - \langle \varepsilon_z \rangle)^2 \right\rangle}. \tag{15}$$

where ε_i and $\langle \varepsilon_i \rangle$ represent the instantaneous and time-averaged strain, respectively.

In Fig. 6 the fluctuations in box size are plotted as a function of time. The change of box shape is due to a slow relaxation of the structure. In order to compute the statistics of fluctuations, these results were used even though equilibrium was not fully reached yet by fitting the slowly changing box sizes to third order polynomials. A third-order polynomial fit is used as it represents the trend of curve quite well. The fluctuation of a quantity is computed as the difference between an instantaneous value minus the value of the polynomial fit at that time such that only the amount of instantaneous fluctuations is taken into account. From these fluctuations, *via* the equations as derived in the Appendix, Poisson's ratio v and elastic modulus E are estimated. We predict from Eq. (15) that Poisson's ratio $v = 0.403$ (±0.048). The error in parenthesis is

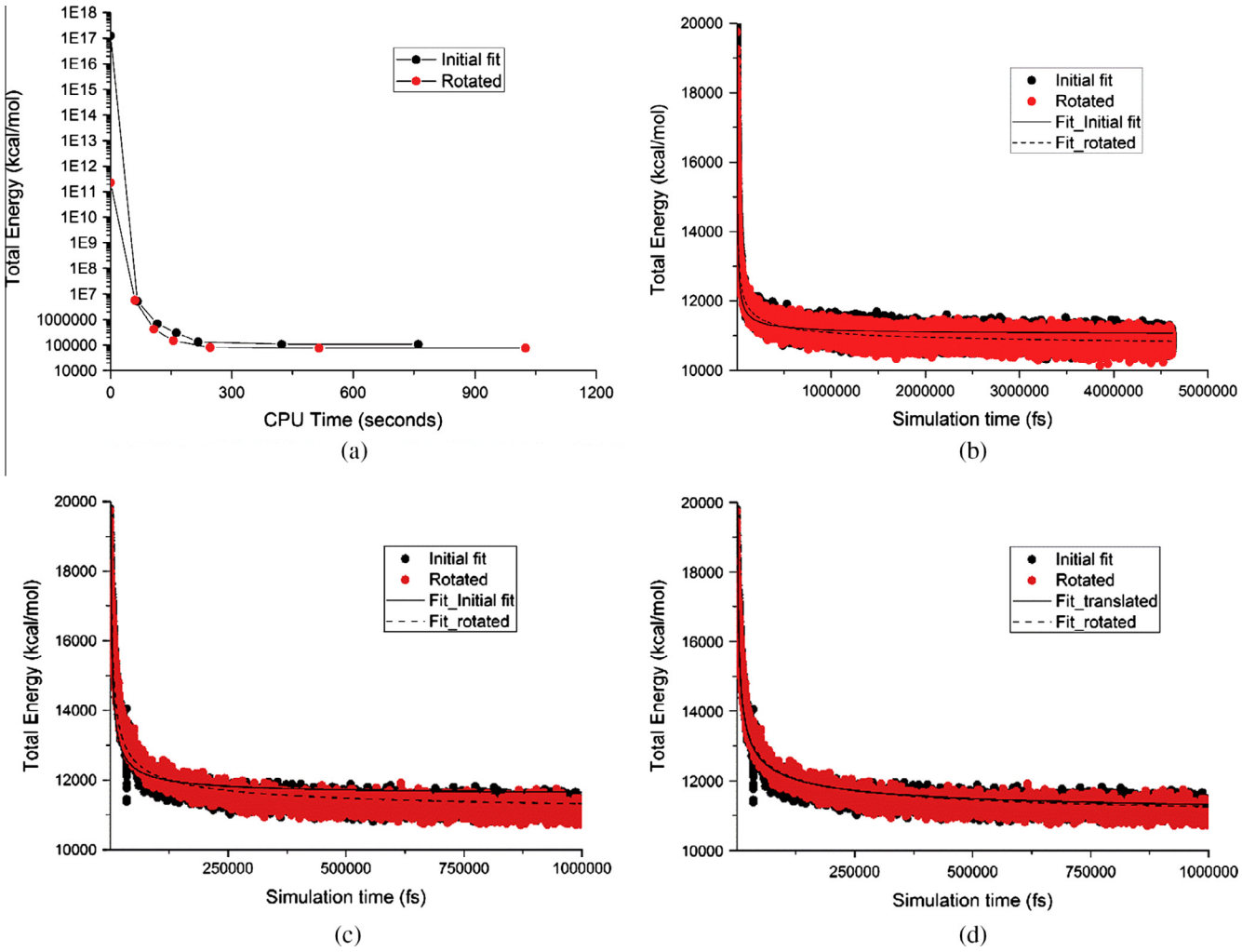

Fig. 4. (a) Total energy as a function of CPU time of the computation for a system fitted from the library of templates (no rotation applied) and for a system with rotated templates. Parallel simulations are performed with Intel® Xeon® X5660 2.80 GHz with 6 cores. (b) Total energies of reverse-mapped structures from initial fit of templates and rotated templates as a function of simulation time. The lines indicate the power law fits in form of $y = ax^b + c$. The fit parameters are $a = 1.26 \times 10^6$, $b = -0.6558$, $c = 1.102 \times 10^4$ for only fitted templates, and $a = 1.879 \times 10^5$, $b = -0.4299$, $c = 1.059 \times 10^4$ for rotation applied case. Consecutively, for the reverse-mapping procedure of initial fit of templates and rotated templates, the power law fit parameters are for (c) $a = 1.062 \times 10^6$, $b = -0.6621$, $c = 1.154 \times 10^4$, and $a = 2.819 \times 10^5$, $b = -0.474$, $c = 1.092 \times 10^4$ (d) $a = 2.37 \times 10^5$, $b = -0.4524$, $c = 1.086 \times 10^4$, and $a = 1.514 \times 10^5$, $b = -0.3973$, $c = 1.063 \times 10^4$.

computed by means of the block averages method [41]. From Eq. (14) we have for the elastic modulus $E = 1.909$ (±0.103) GPa. Moreover, we calculated E from three consecutive blocks of the fitted region of Fig. 6, which resulted in $E = 1.76 \pm 0.18$, 1.92 ± 0.15 and 2.10 ± 0.18 GPa, respectively. Within error, these values are the same, although taken from a decreasing overall trend (first) block, an approximately constant (second) block and an increasing trend (third) block, indicating the validity of the approach. Finally, from Eq. (13), we have for the bulk modulus $B = 4.45$ (±2.39) GPa.

We compare our simulation results of the DGEBA/DETA based epoxy with the available experimental data. Although Poisson's ratio is not so commonly reported and specifically not at the stoichiometric ratio (~95:5 wt. ratio), Possart et al. estimated as 0.39 (±0.10) [42]. For a non-stoichiometric mixture (~90:10 wt. ratio [43]), Poisson's ratio is reported as 0.345 which is in the range of typical values for various epoxy systems 0.3–0.4 [6,44,45].

The elastic modulus values found in literature show a variation depending on the epoxy-amine composition. For example, Grishchuk et al. [46] prepared mixtures at the stoichiometric ratio, measured E by three-point bending tests, and reported $E = 2.8$ (±0.07) GPa. In addition, Aufray and Roche [47] report $E = 2.7$ (±0.1) GPa, also from three-point flexure tests. However, for non-stoichiometric samples (~90:10 wt. ratio), Denq et al. [48] estimated as $E \cong 1.7$ GPa by tensile testing, while Asp et al. [43] measured 2.07 GPa by biaxial testing.

In all, in view of the scarcity of experimental data, our estimation for Poisson's ratio is in good agreement with the reported experimental values in literature. However, our computational prediction for the E modulus is lower than experimental measurements for stoichiometric mixtures. The discrepancy in E modulus may be attributed to the slow relaxation of the cross-linked epoxy structure. The standard fluctuation approach to calculate the Poisson's ratio solely depends on the instantaneous fluctuations of the box length in different dimensions. This represents the instantaneous deformation of the box, and independent of the equilibrium value of the box dimension. On the other hand, as Eq. (14) signifies, the prediction of Young's modulus depends on the equilibrium volume of the box. If the box is not yet relaxed to its equilibrium value, the prediction of Young's modulus is in principle incorrect. As the epoxy is at the near-equilibrium (or quasi-equilibrium) state, this can also be a source of discrepancy between the experimental and simulated values of Young's modulus. We summarize the computed and experimentally reported elastic properties in Table 1.

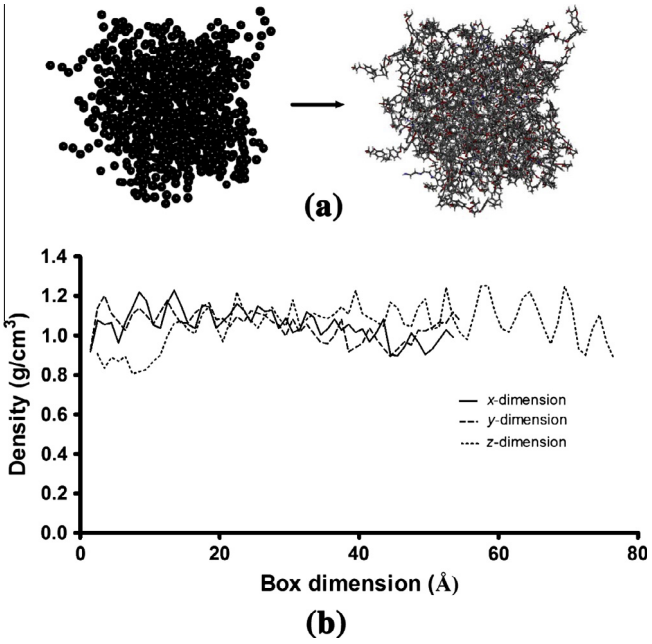

Fig. 5. (a) DPD output coordinates are presented on the left, and the reverse-mapped atomistic structure is on the right. (b) The density profiles plotted in different dimensions of the box.

We calculated Poisson's ratio v and Young's modulus E for the structure obtained from the initial step of the reverse-mapping procedure (that is, using initial fitted coordinates, as described by the first step of Fig. 3) and repeated the same procedure as described above. The calculated values are $v = 0.382$ and $E = 1.80$ GPa, which are lower than the predictions of the full reverse-mapping procedure applied. Therefore, the computational gain in implementing a rotation algorithm is also evident in the calculated properties.

3.3. T_g of bulk epoxy

Another important property for polymers is the glass transition temperature T_g and we attempted to assess its value for bulk epoxy under discussion.

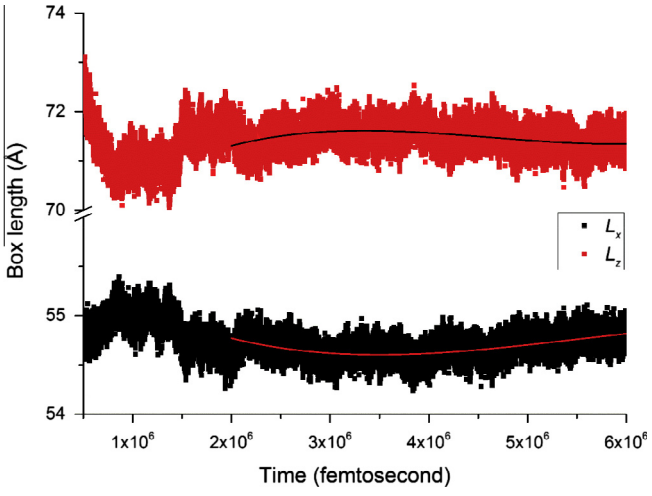

Fig. 6. The fluctuations of the box lengths in x and z dimensions as a function of time. The lines indicate the third order polynomial fit ($y = a + bx + cx^2 + dx^3$) to data with parameters are $a = 55.77$, $b = -7.94 \times 10^{-7}$, $c = 1.67 \times 10^{-13}$, $d = -1.03 \times 10^{-20}$ for L_x, and $a = 68.97$, $b = 1.95 \times 10^{-6}$, $c = -4.58 \times 10^{-13}$, $d = 3.32 \times 10^{-20}$ for L_z.

Table 1
Poisson's ratio v and elastic modulus E for bulk epoxy compared with available experimental values. When available, the experimental error is indicated in brackets. The error for the computed values is estimated with the block averages method [41].

	Poisson's ratio v	Elastic modulus E (GPa)
Experiments	0.39 (±0.10) [42]†	2.9 (±0.3) [42]†
		2.8 (±0.07) [46]†
		2.7 (±0.1) [47]†
	0.345 [43]‡	2.07 [43]‡
		1.7 [48]‡
Simulations	0.403 (±0.048)	1.909 (±0.103)

† Stoichiometric compositions.
‡ Non-stoichiometric compositions.

Fig. 7 shows the volume of the epoxy, demonstrating a clear transition at about 150 °C between two different regions, where the lower temperature region corresponds to the glassy state, and the higher temperature region corresponds to the rubbery state.

The T_g is calculated as the intersection temperature from fitting lines to these upper and lower temperature regions, resulting in 168.1 ± 3.2 °C. Experimentally, the glass transition temperature of DGEBA/DETA is measured as 130 °C, and 135 °C from DSC and DMTA measurements, respectively [46]. Our computed value for T_g is different from the experimental values. There might be a number of reasons for the discrepancy between calculated and experimental values for T_g, such as line fitting error, selection of the force field, relaxation times of cross-linked polymers, the inaccuracy in the experimental measurements, the additive and impurities present in the epoxy in reality and polydispersity. For the comparison of T_g, the cooling rate is of prime importance, shifting T_g to lower temperature using lower cooling rates [49–51]. Experimentally the effect of cooling rate is estimated as 5 °C for a change of cooling rate from 10 °C/min to 1 °C/min [46] corresponding to an order of magnitude. If we assume a similar effect in simulations, the simulated $T_g = 168$ °C (using a cooling rate of 15 °C/500 ps) would have to be corrected to about 113 °C (for a typical experimental cooling rate of 10 °C/min). The effect of cooling rate is somewhat different as predicted by computer simulations for a similar epoxy-amine system. A difference of about 3 °C per order of magnitude is predicted from the William–Landel–Ferry (WLF) equation taking into consideration the correlation between the relaxation times and the cooling rate and reported in [52]. In this case, the corrected T_g would be about 135 °C in our estimation.

We estimate the coefficient of thermal expansion α_T using $\alpha_T = 1/V_0(\partial V/\partial T)_p$, where V_0 is the volume at 300 K and 510 K for

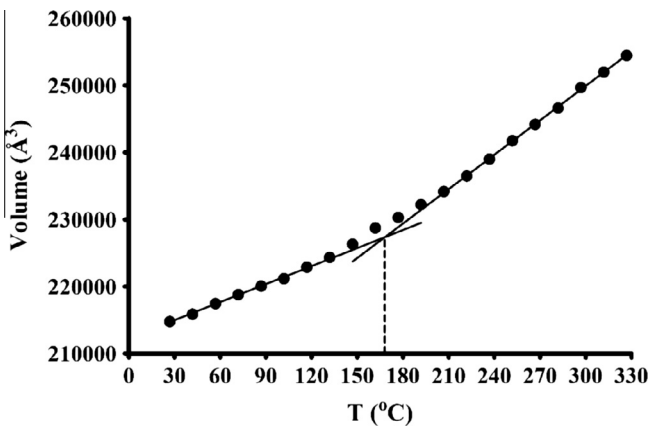

Fig. 7. Volumetric variation of epoxy as a function of the change in temperature.

the glassy and rubbery state, respectively. We use the values in calculating α_T as plotted in Fig. 7. The calculated values of α_T are $3.52(\pm 0.18) \times 10^{-4}$/K for the glassy regime, and $6.72(\pm 0.13) \times 10^{-4}$/K for the rubbery regime. For a rough comparison, experimental values for the corresponding regimes for an example epoxy system are measured as 1.95×10^{-4}/K and 5.79×10^{-4}/K, respectively [53].

4. Conclusions

In this paper coupling of mesoscopic and atomistic scale simulations for material properties is presented. To that purpose we used coordinates of a cross-linked epoxy structure created at the DPD-scale as an input to reverse-mapping. We established a fast and efficient algorithm to insert the atomistic details into the mesoscopic structure which allows performing atomistic simulations from a structure equilibrated at much larger length and time scales as is generally feasible with MD simulations. The algorithm contains various steps to obtain the best alignment between characteristic vectors of consecutive atomistic templates. The reverse-mapping of the atomistic detail was tested by observing the bond length distributions between these templates for a single chain and for a fully cross-linked structure of an epoxy resin. The rotation step implemented in the algorithm provided a better energy minimization of the structure as compared to the structure with non-rotated (randomly oriented) templates.

The reverse-mapped structure was used to compute some characteristic properties of the bulk epoxy. Atomistic simulations were performed using the reverse-mapped structure and the elastic modulus, Poisson's ratio, glass transition temperature and thermal expansion coefficients below and above the glass transition temperature were calculated. A derivation using standard fluctuation theory for computing these properties from the instantaneous box length fluctuations was presented. Moreover, the computed properties were compared with the experimental values reported in the literature. Although some deviations from the experimentally available data were observed, the results are considered to be in agreement. The reasons for these deviations are discussed and regarded as the effect of the slow relaxation of the cross-linked epoxy (quasi-equilibrium), fitting errors, selection of the force field, inaccuracy in the experimental measurements, the additive and/or impurities as well as polydispersity present in the experimental epoxies.

It should be noted that by the use of the parameterization method for DPD interactions developed previously in our group [26], it is ensured that the local specific volumes for a particular bead are consistent with experimental pure liquid specific volumes (in contrast to the conventional parameterization where large deviations can occur). This improved representation of the variable local specific volumes, renders the reverse-mapping of atomistic detail more efficient as these volumes of beads heavily influence the pre-equilibrated bond lengths.

In all, we conclude that the procedures presented in this work will be useful in bridging the computational molecular simulations to the experimentally measured material properties with a fast and straightforward mapping with significant accuracy.

Acknowledgements

The authors are grateful to STW for the financial support for the project number 10121 under the MuST program 'Multi-scale Simulation Techniques'.

Appendix A. Box size fluctuations

To derive an expression for the elastic modulus E and Poisson's ratio ν from simulation result fluctuations, we start with the observation that any probability density in statistical mechanics is proportional to $\exp[-S_{tot}/k_B]$, where S_{tot} is the total entropy, i.e., of the system plus that of the environment. This is sometimes called the Einstein distribution. Using the general thermodynamic relation that the entropy equals the energy of the system E_{sys} minus the Helmholtz energy A_{sys} divided by the temperature, we have

$$S_{sys} = \frac{E_{sys} - A_{sys}}{T}. \tag{16}$$

Since the environment is large, exchange of energy with the system constitutes an infinitesimal change so that it can be assumed that the temperature of the environment does not change. Similarly, when the system changes size, the stresses applied by the environment remain constant. A change of entropy of the environment then equals:

$$\Delta S_{env} = \frac{\Delta E_{env} - \Delta W_{env}}{T} \tag{17}$$

where ΔE_{env} is the change of energy of the environment and ΔW_{env} the reversible mechanical work performed on the environment. This work is performed by the system and equals $W_{env} = -V\sum_i \varepsilon_i \sigma_i$, relative to the undeformed system. If the two entropies are added, and conservation of energy is used ($E_{sys} + E_{env} =$ constant), we find, using $\boldsymbol{L} = \{N, T, L_x, L_y, L_z\}$ as abbreviation,

$$S_{tot}(\boldsymbol{L}) = S_0 - \frac{A_{sys}(\boldsymbol{L}) - V\sum_i \varepsilon_i \sigma_i}{T} \tag{18}$$

The probability distribution of box sizes can now be computed from this, using $\beta = 1/k_B T$, as

$$p(\boldsymbol{L}) = Z^{-1} \exp\left[-\beta\left(A_{sys}(\boldsymbol{L}) - V\sum_i \varepsilon_i \sigma_i\right)\right], \tag{19}$$

where for proper normalization we need the isobaric-isothermal partition function

$$Z(\boldsymbol{L}) = \iiint \exp\left[-\beta\left(A_{sys}(\boldsymbol{L}) - V\sum_i \varepsilon_i \sigma_i\right)\right] d\boldsymbol{L} \tag{20}$$

The Gibbs energy is related to this partition function as

$$G = -k_B T \ln\ Z \tag{21}$$

One way to check the consistency is to evaluate its derivatives. For example,

$$\begin{aligned}
\frac{\partial G}{\partial \sigma_i} &= -k_B T\ Z^{-1} \frac{\partial Z}{\partial \sigma_i} \\
&= -k_B T\ Z^{-1} \iiint \frac{\partial}{\partial \sigma_i} \exp\left[-\beta\left(A_{sys}(\boldsymbol{L}) - V\sum_i \varepsilon_i \sigma_i\right)\right] d\boldsymbol{L} \\
&= -Z^{-1} \iiint V\varepsilon_i \exp\left[-\beta\left(A_{sys}(\boldsymbol{L}) - V\sum_i \varepsilon_i \sigma_i\right)\right] d\boldsymbol{L} \\
&= -V \iiint \varepsilon_i p(\boldsymbol{L}) d\boldsymbol{L} = -V\langle \varepsilon_i \rangle
\end{aligned} \tag{22}$$

This result corresponds to the expected thermodynamic relation (see Eq. (10)). Now, all is set to derive the main result, namely,

$$\begin{aligned}
\frac{\partial^2 G}{\partial\sigma_i\partial\sigma_j} &= -k_BT\left(Z^{-1}\frac{\partial^2 Z}{\partial\sigma_i\partial\sigma_j} - \left(Z^{-1}\frac{\partial Z}{\partial\sigma_i}\right)\left(Z^{-1}\frac{\partial Z}{\partial\sigma_j}\right)\right)\\
Z^{-1}\frac{\partial^2 Z}{\partial\sigma_i\partial\sigma_j} &= Z^{-1}\iiint \frac{\partial^2}{\partial\sigma_i\partial\sigma_j}\exp\left[-\beta\left(A_{sys}(\boldsymbol{L}) - V\sum_i \varepsilon_i\sigma_i\right)\right]d\boldsymbol{L}\\
&= \left(\frac{V}{k_BT}\right)^2 Z^{-1}\iiint \varepsilon_i\varepsilon_j\exp\left[-\beta\left(A_{sys}(\boldsymbol{L}) - V\sum_i \varepsilon_i\sigma_i\right)\right]d\boldsymbol{L}\\
&= \left(\frac{V}{k_BT}\right)^2\iiint \varepsilon_i\varepsilon_j p(\boldsymbol{L})d\boldsymbol{L} = \left(\frac{V}{k_BT}\right)^2\langle\varepsilon_i\varepsilon_j\rangle\\
\frac{\partial^2 G}{\partial\sigma_i\partial\sigma_j} &= -\frac{V^2}{k_BT}\langle(\varepsilon_i - \langle\varepsilon_i\rangle)(\varepsilon_j - \langle\varepsilon_j\rangle)\rangle
\end{aligned} \tag{23}$$

When we equate these relations to the thermodynamic relations of Eq. (12), we find that

$$\begin{aligned}
E^{-1} &= \frac{\overline{V}}{k_BT}\langle(\varepsilon_i - \langle\varepsilon_i\rangle)^2\rangle,\ i = x,\ y \text{ or } z,\\
-\nu E^{-1} &= \frac{\overline{V}}{k_BT}\langle(\varepsilon_i - \langle\varepsilon_i\rangle)(\varepsilon_j - \langle\varepsilon_j\rangle)\rangle,\ i \neq j
\end{aligned} \tag{24}$$

In the simulations that are presented, the x and y dimensions of the simulation box are coupled, such that they have equal strain and equal stress, i.e., $\varepsilon_x = \varepsilon_y = \varepsilon_w$ and $\sigma_x = \sigma_y = \sigma_w$. Differentiating the Gibbs energy with respect to σ_w, keeping σ_z fixed, we find

$$\begin{aligned}
\left.\frac{\partial^2 G}{\partial\sigma_w^2}\right|_{\sigma_z} &= \frac{\partial^2 G}{\partial\sigma_x^2} + 2\frac{\partial^2 G}{\partial\sigma_x\partial\sigma_y} + \frac{\partial^2 G}{\partial\sigma_y^2} = -\frac{\overline{V}\ (2-2\nu)}{E}\\
\frac{\partial^2 G}{\partial\sigma_w\partial\sigma_z} &= \frac{\partial^2 G}{\partial\sigma_x\partial\sigma_z} + \frac{\partial^2 G}{\partial\sigma_y\partial\sigma_z} = \frac{2\overline{V}\nu}{E}
\end{aligned} \tag{25}$$

and thus to

$$\begin{aligned}
-\nu E^{-1} &= \frac{\overline{V}}{k_BT}\langle(\varepsilon_w - \langle\varepsilon_w\rangle)(\varepsilon_z - \langle\varepsilon_z\rangle)\rangle,\\
E^{-1} &= \frac{\overline{V}}{k_BT}\langle(\varepsilon_z - \langle\varepsilon_z\rangle)^2\rangle,
\end{aligned} \tag{26}$$

Upon dividing the two last relations in Eq. (26), we obtain the expression for Poisson's ratio, which is the same relation as reported Falcioni et al. [54], namely

$$\nu = -\frac{\langle(\varepsilon_w - \langle\varepsilon_w\rangle)(\varepsilon_z - \langle\varepsilon_z\rangle)\rangle}{\langle(\varepsilon_z - \langle\varepsilon_z\rangle)^2\rangle}. \tag{27}$$

References

[1] D. Frenkel, B. Smit, Understanding Molecular Simulation: From Algorithms to Applications, Academic Press, California, London, 2002.
[2] K.S. Khare, R. Khare, Macromol. Theor. Simul. 21 (2012) 322.
[3] H. Liu, M. Li, Z.Y. Lu, Z.G. Zhang, C.C. Sun, T. Cui, Macromolecules 44 (2011) 8650.
[4] S. Yu, S. Yang, M. Cho, Polymer 50 (2009) 945.
[5] P.V. Komarov, Y.T. Chiu, S.M. Chen, P.G. Khalatur, P. Reineker, Macromolecules 40 (2007) 8104.
[6] C.F. Wu, W.J. Xu, Polymer 47 (2006) 6004.
[7] H. Yagyu, Y. Hirai, A. Uesugi, Y. Makino, K. Sugano, T. Tsuchiya, O. Tabata, Polymer 53 (2012) 4834.
[8] R.D. Groot, P.B. Warren, J. Chem. Phys. 107 (1997) 4423.
[9] P.J. Hoogerbrugge, J.M.V.A. Koelman, Europhys. Lett. 19 (1992) 155.
[10] G. Kacar, E.A.J.F. Peters, G. de With, Soft Matter 9 (2013) 5785.
[11] G. Kacar, E.A.J.F. Peters, G. de With, J. Phys. Chem. C 117 (2013) 19038.
[12] L.T. Yan, E. Maresov, G.A. Buxton, A.C. Balazs, Soft Matter 7 (2011) 595.
[13] J. Baschnagel, K. Binder, P. Doruker, A.A. Gusev, O. Hahn, K. Kremer, W.L. Mattice, F. Muller-Plathe, M. Murat, W. Paul, S. Santos, U.W. Suter, V. Tries, Adv. Polym. Sci. 152 (2000) 41.
[14] C. Peter, K. Kremer, Soft Matter 5 (2009) 4357.
[15] A. Ghanbari, M.C. Bohm, F. Muller-Plathe, Macromolecules 44 (2011) 5520.
[16] G. Santangelo, A. Di Matteo, F. Muller-Plathe, G. Milano, J. Phys. Chem. B 111 (2007) 2765.
[17] I.F. Thorpe, J. Zhou, G.A. Voth, J. Phys. Chem. B 112 (2008) 13079.
[18] B. Hess, S. Leon, N. van der Vegt, K. Kremer, Soft Matter 2 (2006) 409.
[19] A.J. Rzepiela, L.V. Schafer, N. Goga, H.J. Risselada, A.H. De Vries, S.J. Marrink, J. Comput. Chem. 31 (2010) 1333.
[20] T.A. Wassenaar, K. Pluhackova, R.A. Böckmann, S.J. Marrink, D.P. Tieleman, J. Chem. Theor. Comp. (2013) 676.
[21] D.N. Theodorou, U.W. Suter, Macromolecules 19 (1986) 139.
[22] M. Parrinello, A. Rahman, J. Chem. Phys. 76 (1982) 2662.
[23] H.B. Callen, Thermodynamics and an Introduction to Thermostatistics, second ed., John Wiley & Sons Inc., New York and London, 1985 (Ch. 19 in second ed. and see also first ed. Ch. 15, 1960).
[24] H. Makki, K.N. Adema, E.A.J.F. Peters, J. Laven, L.G. van der Ven, R.A. van Benthem, G. de With, Polym. Degr. Stab. 105 (2014) 68.
[25] R.D. Groot, K.L. Rabone, Biophys. J. 81 (2001) 725.
[26] G. Kacar, E.A.J.F. Peters, G. de With, EPL 102 (2013) 40009.
[27] S. Plimpton, J. Comput. Phys. 117 (1995) 1.
[28] H. Sun, S.J. Mumby, J.R. Maple, A.T. Hagler, J. Am. Chem. Soc. 116 (1994) 2978.
[29] H. Sun, J. Phys. Chem. B 102 (1998) 7338.
[30] W.G. Hoover, Phys. Rev. A 31 (1985) 1695.
[31] S. Nose, J. Chem. Phys. 81 (1984) 511.
[32] M. Parrinello, A. Rahman, J. Appl. Phys. 52 (1981) 7182.
[33] T. Darden, D. York, L. Pedersen, J. Chem. Phys. 98 (1993) 10089.
[34] G. Kacar, Materials Science and Engineering, M.Sc. Thesis, Sabanci University, Istanbul, 2008.
[35] G. Kacar, C. Atilgan, A.S. Ozen, J. Phys. Chem. C 114 (2010) 370.
[36] W.A. Dollase, Acta Crystallogr. A, A 30 (1974) 513.
[37] E.H. Thompson, An Introduction to the Algebra of Matrices with Some Applications, Univ. of Toronto Press, 1969.
[38] E.H. Moore, Bull. Am. Math. Soc. 26 (1920) 394.
[39] R. Penrose, Proc. Camb. Philos. Soc. 51 (1955) 406.
[40] G. Kacar, E.A.J.F. Peters, G. de With, Soft Matter 9 (2013) 5785.
[41] B. Hess, J. Chem. Phys. 116 (2002) 209.
[42] G. Possart, M. Presser, S. Passlack, P.L. Geiss, M. Kopnarski, A. Brodyanski, P. Steinmann, Int. J. Adhes. Adhes. 29 (2009) 478.
[43] L.E. Asp, L.A. Berglund, Exp. Mech. 37 (1997) 96.
[44] I.P. Aspin, J.M. Barton, G.J. Buist, A.S. Deazle, I. Hamerton, B.J. Howlin, J.R. Jones, J. Mater. Chem. 4 (1994) 385.
[45] S.P.M. Noijen, O. van der Sluis, P.H.M. Timmermans, G.Q. Zhang, Microelectron. Reliab. 49 (2009) 1315.
[46] S. Grishchuk, Z. Mbhele, S. Schmitt, J. Karger-Kocsis, Exp. Polym. Lett. 5 (2011) 273.
[47] M. Aufray, A.A. Roche, J. Adhes. Sci. Technol. 20 (2006) 1889.
[48] B.L. Denq, Y.S. Hu, L.W. Chen, W.Y. Chiu, T.R. Wu, J. Appl. Polym. Sci. 74 (1999) 229.
[49] J.L. Barrat, J. Baschnagel, A. Lyulin, Soft Matter 6 (2010) 3430.
[50] J. Buchholz, W. Paul, F. Varnik, K. Binder, J. Chem. Phys. 117 (2002) 7364.
[51] A. Soldera, N. Metatla, Phys. Rev. E 74 (2006) 061803.
[52] C.Y. Li, A. Strachan, Polymer 52 (2011) 2920.
[53] K.M.B. Jansen, L. Wang, D.G. Yang, C. van't Hof, L.J. Ernst, H.J.L. Bressers, G.Q. Zhang, Elect. Comp. C (2004) 890.
[54] M. Falcioni, M.J. Bowick, E. Guitter, G. Thorleifsson, Europhys. Lett. 38 (1997) 67.